


Mesoporous Silica Hybridized With Gadolinium(III) Nanoplatfom for Targeted Magnetic Imaging–Guided Photothermal Breast Cancer Therapy

Dose-Response:
An International Journal
January-March 2020: 1-10
© The Author(s) 2020
Article reuse guidelines:
sagepub.com/journals-permissions
DOI: 10.1177/1559325820902314
journals.sagepub.com/home/dos



Longqing Wang¹ and Xiaofeng Sun² 

Abstract

Achieving drug target accumulation in antitumor tissue, simultaneous diagnostic imaging, and optimal release behavior with treatment needs a best chemotherapy procedure involving receptive switch of drug delivery. Constructed on mesoporous silica nanoparticles, which are crossed with multiscale charming nanoparticles for magnetic resonance imaging (MRI)-aided and alternate magnetic field (AMF) response chemotherapy for breast cancer, we report in this work the assembly of a new theranostics drug conveyance process. Hydrothermal processes (gadolinium(III) oxide nanoparticles [Gd-NPs]) and heat decomposition process (radical size uFe-NPs) were used to prepare superparamagnetic Gd-NPs with multiscale sizes. Gadolinium(III) oxide nanoparticles act as an AMF-responsive heat mediator, while ultra-Fe nanoparticles (uFe-NPs) act as an MRI T₂ contrast mediator. Nanoparticles of the mesoporous silica with radially oriented mesochannels were further grown in situ on the surfaces of the Gd-NPs, and the uFe-NPs anticancer drug doxorubicin can be easily incorporated in the mesochannels. To provide better targeting capabilities for the as-synthesized biotin-loaded nanohybrids, the particle surfaces are updated with biotin (Bt). This optimized drug conveyance method based on nanocomposites of SiO₂ demonstrated great efficiency of medication charging and receptive properties of AMF stimulus release. However, tests of MRI in vitro showed an outstanding contrast effect in MRI with a high stimulation quality (299 mM⁻¹ s⁻¹). In contrast, the study of in vitro cytotoxicity assessment revealed that an MRI-directed stimulus-mediated theranostics tool can be used as a drug conveyance device to efficiently treat breast cancer.

Keywords

mesoporous, gadolinium(III) oxide, breast cancers, MR imaging

Introduction

Since the Food and Drug Administration authorized the first anticancer drug for the diagnosis of human cancer, chemotherapy has been accepted as the most common type of treatment for all stages of cancer, including patients with early-stage illness and full-resection patients.¹⁻⁴ Nevertheless, following a growing list of highly effective chemotherapy agents, for instance, docetaxel, vincristine, topotecan, pemetrexed, paclitaxel, and irinotecan, extreme side effects of therapy remain the major challenges during care due to excess dosage and unselective conveyance of chemotherapy mediators.⁵⁻⁸ Nanotechnology-based drug delivery systems facilitate administration mechanisms for the effective conveyance of medications to grazes and targeting sites to prevent inadequate management due to low-dose and overdose poisonousness quality. However, when these conveyance processes

demonstrated release performance, drug concentrations might be consistently delivered in the appropriate therapeutic sort. Different drug conveyance processes, such as liposomes, hydrogels, dendritic polymers, nanocapsules micelles,

¹ Department of Gastrointestinal and Mammary Surgery, General Hospital of Fushun Liaoning Health Industry Group, Fushun, China

² Department of Ultrasound, Central Hospital of Wuhan, Tongji Medical College, Huazhong University of Science and Technology, Wuhan, China

Received 24 November 2019; received revised 25 December 2019; accepted 31 December 2019

Corresponding Author:

Xiaofeng Sun, Department of Ultrasound, Central Hospital of Wuhan, Tongji Medical College, Huazhong University of Science and Technology, No. 14, Gusaoshu Road, Jiangnan District, Wuhan 430000, China.
Email: sun_xiaofeng@yahoo.com



Creative Commons Non Commercial CC BY-NC: This article is distributed under the terms of the Creative Commons Attribution-NonCommercial 4.0 License (<https://creativecommons.org/licenses/by-nc/4.0/>) which permits non-commercial use, reproduction and distribution of the work without further permission provided the original work is attributed as specified on the SAGE and Open Access pages (<https://us.sagepub.com/en-us/nam/open-access-at-sage>).

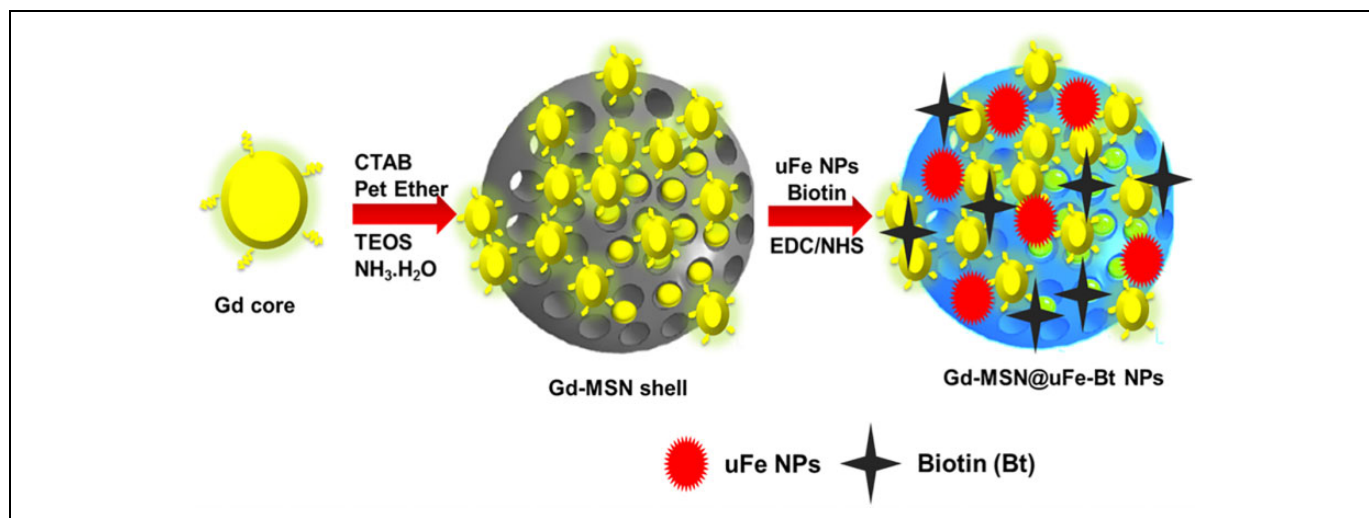


Figure 1. A graphical sketch of the synthesized of Gd-MSN@uFe-Bt-NPs and magnetic resonance imaging-guided breast cancer photodynamic therapy.

nanospheres, and liquid crystals, have been effectively established over the past decade for effective inert or energetic directing conveyance strategies. Although every system has its individual compensation, numerous significant limitations often disturb its additional application. Owing to the high-density lipoproteins, charity such as liposome and micelles might affect from reduced chemical constancy. In the meantime, toxicity difficulties are the key problems to the application of nanospheres, hydrogels, and polymers due to *in vivo* degradation difficulties, while dendrimers are imperfect due to their rapid removal by the kidneys and liver.⁹⁻¹¹

Mesoporous silica nanoparticles (MSNs) have fascinated considerable consideration in drug conveyance in the research field, as both materials display adjustable pore size, chemical inertia, thermal stability, large surface area, excellent biodegradability, and biocompatibility.¹²⁻¹⁵ Their porous interior and huge surface make these resources outstanding reservoirs for the delivery of hydrophobic medications and also their variable pore sizes can be designed to particularly insert different anti-tumor drug molecules of interest. Further, the simple synthesis procedure helps us to receive enhanced shapes and sizes for extreme uptake into tumor cells.¹⁶⁻¹⁹ Furthermore, the easy modification of the mesoporous silica surface is possible to design active-targeting and stimulus-responsive drug conveyance process. The medication transport process must be explicit and time-controlled so as to accomplish exact disease chemotherapy. Contrasted with the inactive focusing on gave by the upgraded porousness and maintenance impact (EPR impact), dynamic focusing on techniques, for example, including an immune response, bearer protein, or ligand to the medication conveyance framework, would enable it to gather at the objective area, accomplishing high adequacy with low dose and low symptoms and poisonous quality. Controlled arrival of medications from conveyance frameworks can be actuated by different interior or outer upgrades, for example,

temperature, light, electrical field, elective attractive field (alternate magnetic field, AMF), pH, redox, catalyst movement, and mechanical power. Among these, AMF delicate frameworks, which can be incited by reconciliation with supermagnetic iron oxide nanoparticles, have high potential for medicating discharge because of their well-being, high entrance profundity, and absence of radio harmfulness. Also, supermagnetic iron oxide nanoparticles stacked in the medication conveyance framework can be utilized as a T₂-weighted magnetic resonance imaging (MRI) differentiate specialist to assess the focusing on.²⁰⁻²³ The plan of a proficient conveyance framework with high medication charging limit, dynamic focusing on, and improved reaction conduct, alongside a simultaneous treatment symptomatic procedure, is in this manner significant for effective disease treatment.

In this study, we document a new drug conveyance process based on MSNs, which is hybridized with multiscale MNPs, for MRI-guided breast cancer chemotherapy (Figure 1). Multiscale size superparamagnetic iron oxide (gadolinium(III) oxide nanoparticle, Gd-NPs) has been prepared using a hydrothermal technique (Gd-NPs) and a thermal decay method (uFe-NPs), Gd-NPs act as an AMF-responsive intermediary, and uFe-NPs act as a T₂-contrast agent for MRI. Mesoporous silica sphere with radially directed mesochannels was further developed *in situ* on the surfaces of Gd-NPs, and both uFe-NPs and biotin, an anticancer drug, can be readily integrated into the mesochannels (Gd-MSN@uFe-Bt-NPs) to provide as-synthesized biotin loaded with excellent targeting ability to receive the final Gd-MSN@uFe-Bt-NPs. The results show that as-synthesized Gd-MSN@uFe-Bt-NPs have shown the MRI contrast effect of drug delivery efficiency and same size. Further, *in vitro* anticancer analysis examination has shown that Gd-MSN@uFe-Bt-NPs are an outstanding drug conveyance mechanism with excellent impending as an MRI-aided stimuli-response drug conveyance theranostic tool for successful active breast cancer chemotherapy.

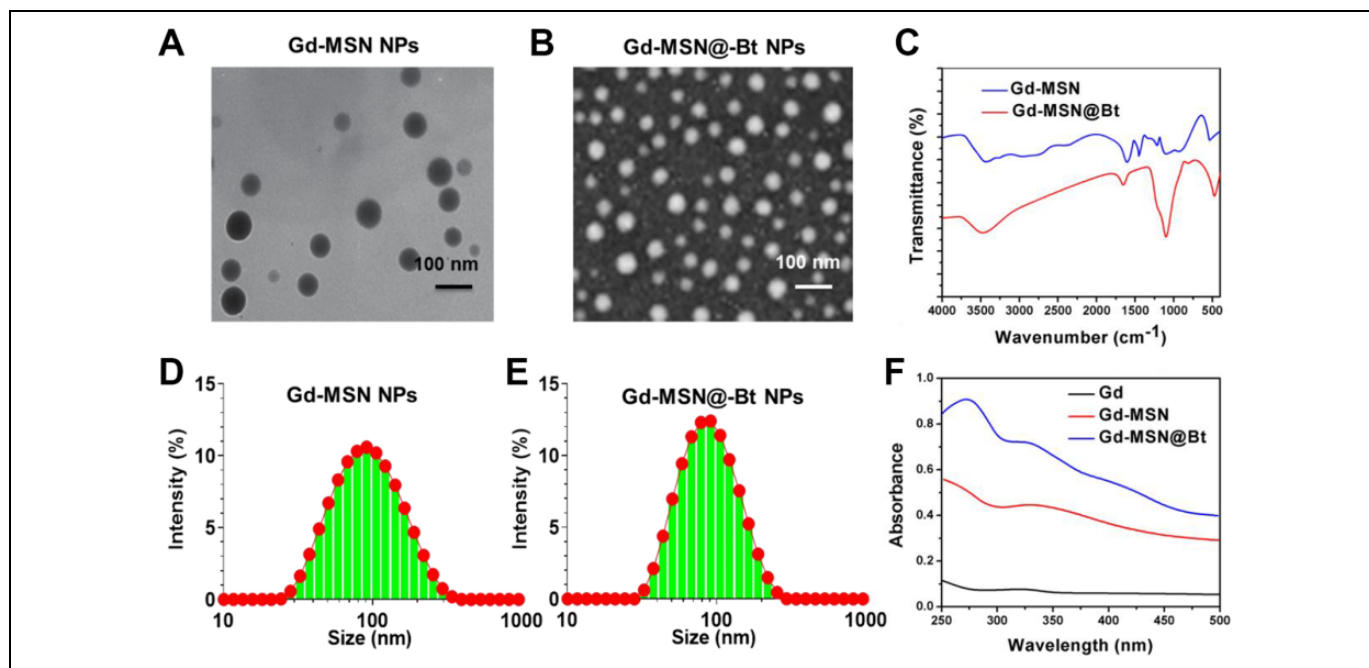


Figure 2. A and B, A transmission electron microscopy image. Scale bar is 100 nm. C, Infrared spectroscopy image of Gd-MSN NPs and Gd-MSN@uFe-Bt-NPs. D and E, DLS of Gd-MSN NPs and Gd-MSN@uFe-Bt-NPs. F, UV-VIS image of Gd, Gd-MSN NPs, and Gd-MSN@uFe-Bt-NPs.

Results and Discussion

Synthesis and Characterization of Gd-MSN@uFe-Bt-NPs

A simple soft-template method is shown in Figure 2 for synthesizing uniform Gd-MSN@uFe-Bt-NPs. The first was the single-pot hydrothermal method used for processing Gd-NPs. Both the transmission electron microscopy (TEM) and scanning electron microscopy (SEM) images show the irregular spherical shape of the as-prepared Gd-NPs of a uniform diameter of ~ 93 nm. The soft models for Gd-NPs synthesis were then used as the Gd-NH₂ MSN. As shown in Figure 2A and B, the NPs have a medium size of ~ 113 nm and consists of an irregular, radially oriented mesostructured, which is further confirmed by the TEM microscopy.²⁴⁻²⁶ Continuous radial mesostructure suggests that this kind of mesoporous Gd-MSN-NPs can allow guest nanoparticles or molecules, such as anticancer therapies, to be loaded or adsorbed and published. Eventually, Gd-MSN@Bt-NPs and Gd-MSN@uFe-Bt-NPs were synthesized by modifying the surfaces with biotin and using a cross-linker to load uFe-NPs in the radial mesonanostructure of Gd-MSN-NPs. After APTES was conjugated on the outer surface of the Gd-MSN-NPs to get Gd-MSN-NH₂-NPs, EDC can simply react with the $-\text{COOH}$ groups of biotin, which was effortlessly removed from the reaction mixture by the attack of nucleophile from the $-\text{NH}_2$ groups of the preprepared Gd-MSN-NH₂. Figure 2 evidently demonstrates that biotin blocked the nanostructure of Gd-MSN-Bt-NPs, resulting in a rougher surface relative to the Gd-MSN-NPs. The final Gd-MSN@uFe-Bt-NPs have been obtained after stacking with uFe-NPs in the radial nanostructures. Further, the variations

in hydrodynamic diameter of Gd-MSN-NPs to get Gd-MSN-NH₂-NPs during synthesis were recorded and are shown in Figure 2D and E.

UV-VIS absorbance spectroscopy and Fourier-transform infrared (FT-IR) spectroscopy were performed for Bt, Gd-MSN@uFe-NPs and Gd-MSN@uFe-Bt-NPs in order to further test the Bt on the Gd-MSN@uFe-Bt-NPs (Figure 2C). The Gd-MSN@uFe-Bt-NPs displayed an important peak at approximately 360 nm corresponding to the Bt UV spectrum (Figure 2F).²⁷ Furthermore, due to the presence of the $-\text{C}[\text{double bond, length as m-dash}]-\text{O}$ bond at 1679 cm^{-1} , the FT-IR results indicate a positive Bt modification, showing the loading of the uFe-NPs and Bt encapsulation. The high-resolution SEM (HR-SEM) descriptions evidently establish the nanostructure morphology of the uFe-NPs and the amorphous MSN structure of the Gd-MSN@uFe-Bt-NPs (Figure 3), which was confirmed by the mapping of the corresponding element. In addition, the HR-SEM energy dispersive spectroscopy (EDS) image of Gd-MSN@uFe-Bt-NPs shows EDS elemental maps for the elements C K α , Gd K α , Si K α , O K α , and Fe K α .

The In Vitro Cytotoxicity and Cellular Uptake

As it is well established, a drug delivery system's biocompatibility and cytotoxicity are of prodigious importance for its presentation in the field of medicinal chemistry. The in vitro cytotoxicity of Gd-MSN@uFe-Bt-NPs against the L929 cell line was therefore discussed utilizing the CCK assay method. The L929 cells showed the high cell viability of more than 95% after incubated for 24 and 48 hours with a high concentration of

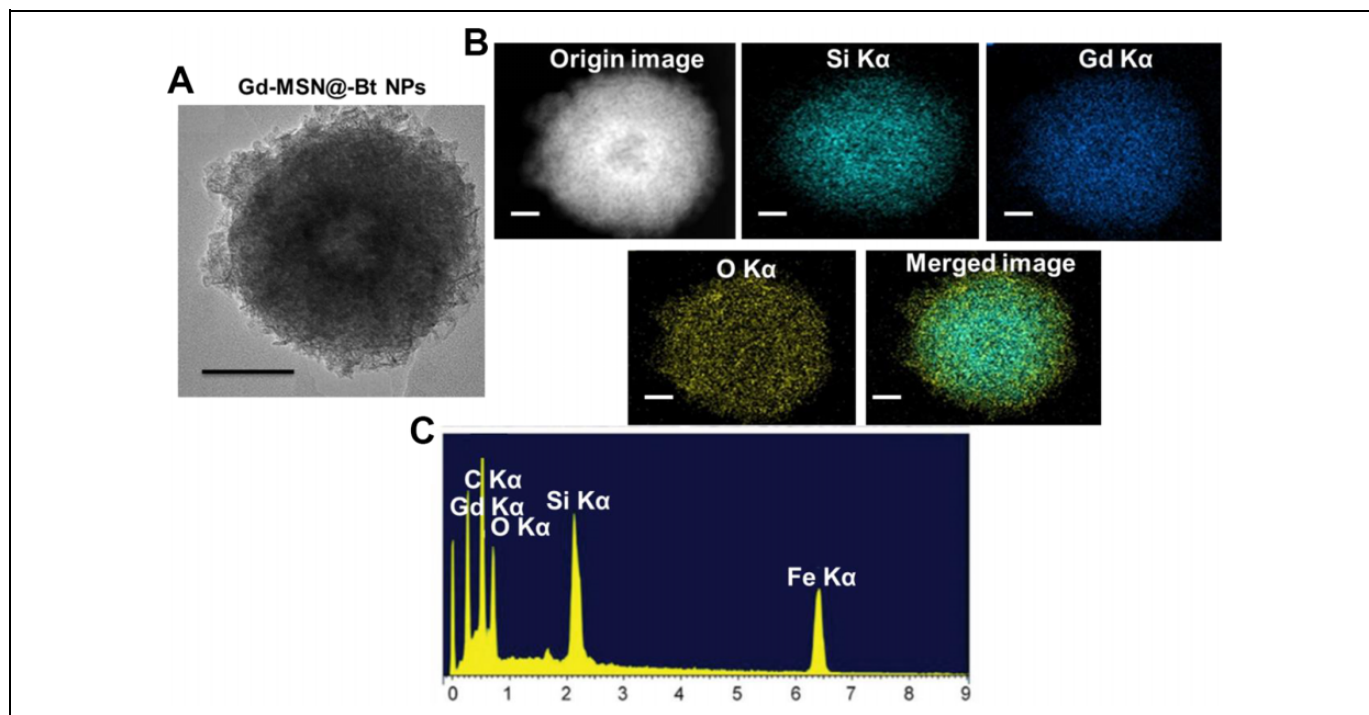


Figure 3. A, Scanning electron microscopy images of Gd-MSN@uFe-Bt-NPs. B, High-resolution scanning electron microscopy image of Gd-MSN@uFe-Bt-NPs. C, Energy dispersive spectroscopy elemental maps for the elements C K α , Gd K α , Si K α , O K α , and Fe K α . Scale bar is 50 nm.

Gd-MSN@uFe-Bt-NPs of $200 \mu\text{g}\cdot\text{mL}^{-1}$ (Figure 4). Although the cell viability decreased slightly after 48 hours of incubation at a concentration of $500 \mu\text{g}\cdot\text{mL}^{-1}$, the cell viability remained as high as 85%, suggesting that the Gd-MSN@uFe-Bt-NPs can be utilized as an effective drug conveyance device. The outstanding cellular uptake results obtainable by drug delivery systems' active directing approaches are an actual method to improve the conveyance efficacy and outcome of chemotherapy. A confocal laser scanning microscopy was used to investigate the cell uptake of DiI-loaded Gd-MSN@uFe-Bt-NPs. Figure 5 shows the growing number of nanoparticles adopted in MCF-7 breast cancer cells by different cultivation periods (Figure 5). Clearly, the efficiency of cell uptake for Gd-MSN@uFe-Bt-NPs was much lower than initial uptake, which suggests that Bt can improve the efficacy of cellular uptake of Gd-MSN@uFe-Bt-NPs through the biotin receptor. Further, the cellular uptake efficiency was confirmed by inductively coupled plasma-mass spectrometry (ICP-MS; Figure 4). The different Fe concentrations (5, 10, 15, 20, and $30 \mu\text{g}/\text{mL}$). The CLSM and ICP-MS results are revealed that the Gd-MSN@uFe-Bt-NPs are effectively uptaken by the MCF-7 cells.

In Vitro Cytotoxicity

The cytotoxic effects of Gd-MSN@uFe-Bt-NPs were tested against MCF-7 cells with or without AMF treatment. The results (Figure 4) indicate that Gd-MSN@uFe-Bt-NPs exhibited duration-dependent inhibition of cell proliferation

associated with an untreated cells group. Gd-MSN@uFe-Bt-NPs revealed higher cytotoxicity to MCF-7 cancer cells. Therefore, further biotin within the cells would be released, causing additional cell death. Outstandingly, for the group of Gd-MSN@uFe-Bt-NPs exposed to AMF ($14.02 \text{ kA}\cdot\text{m}^{-1}$, 279 kHz) for 15 minutes, a further effective anticancer consequence was observed with a less cell viability of 45% after 48 hours of incubation associated with 60% deprived of the revelation of the AMF. Hence, the results are displayed that the Gd-MSN@uFe-Bt-NPs show high potential of cancer tissue targeting and improving in vivo chemotherapy.

In Vitro MRI Analysis

To assess the T_2 -signal MRI difference outcome of the Gd-MSN@uFe-Bt-NPs, a 3.0 T full MR imager was applied to get T_2 -signal MR images of the Gd-MSN@uFe-Bt-NPs deferred in DI water with altered (iron) Fe meditations of 0.026, 0.029, 0.032, 0.036, and 0.039 mM. The Fe meditation of the Gd-MSN@uFe-Bt-NPs was regulated by ICP-optical emission spectrometry. As shown in Figure 6, Gd-MSN@uFe-Bt-NPs persuaded a dim gesture improvement in a dose-dependent method. By snowballing Fe meditation, sturdier gestures (dim signal) were found, which was additionally confirmed by the crosswise relaxivity parameter (r_2). The r_2 value of the Gd-MSN@uFe-Bt-NPs was $299 \text{ mM}^{-1}\cdot\text{s}^{-1}$ in terms of Fe, representing that the Gd-

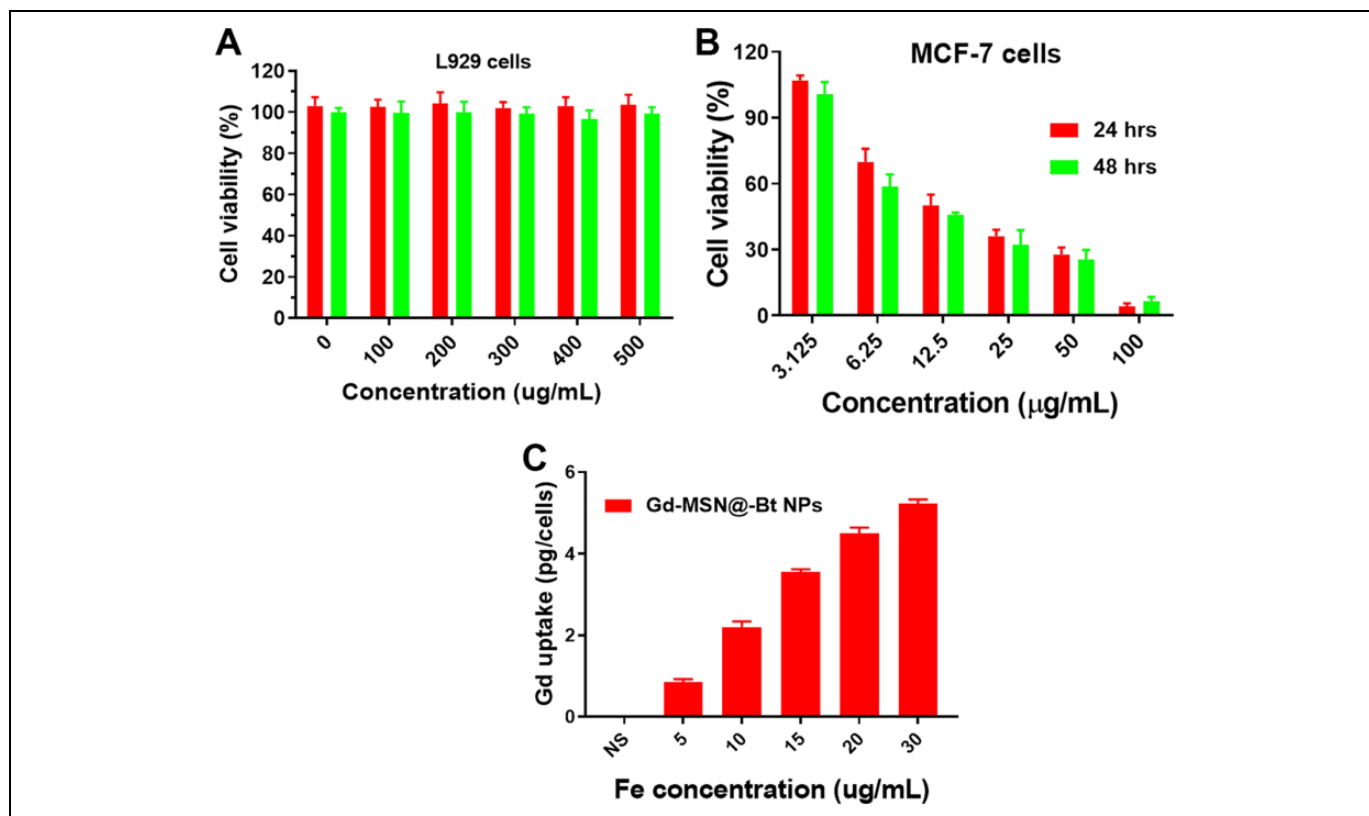


Figure 4. A, The in vitro cell viability of L929 cells after incubation with various concentrations (0, 100, 200, and 500 µg/mL) of Gd-MSN@uFe-Bt-NPs for 24 and 48 hours. B, The in vitro cell viability of MCF-7 cells incubated with Gd-MSN@uFe-Bt-NPs at concentrations of 3.125, 6.25, 12.5, 50, and 100 µg/mL for 24 and 48 hours. C, Cellular uptake of Gd-MSN@uFe-Bt-NPs.

MSN@uFe-Bt-NPs display countless possibility to act as an MRI contrast for using T_2 signals of cancers.

In Vitro Infrared Thermal Imaging

The real-time temperature changes upon irradiation were examined using an infrared (IR) thermal imaging camera. The temperature of the Gd-MSN@uFe-Bt-NPs suspension was rapidly increased over 36°C under irradiation for 2, 4, 6, and 8 minutes and was up to 50°C after 8 minutes (Figure 7). However, the temperature of phosphate-buffered saline was slowly increased to 36°C upon irradiation for 10 minutes. To observe the photothermal conversion effect under laser irradiation, 50, 100, and 150 µg/mL of the Gd-MSN@uFe-Bt-NPs dispersion ($1.0 \times 10^4 \text{ mol}\cdot\text{L}^{-1}$) was stored in vials. The phenomenon meant that Gd-MSN@uFe-Bt-NPs can rapidly convert light energy into heat energy, which was mainly attributed to the Gd-enhanced character of Gd-MSN@uFe-Bt-NPs. The excellent photothermal conversion of the Gd-MSN@uFe-Bt-NPs hybrid enabled its application as a 2-photon photothermal therapeutic agent. After the irradiation, the relative Fe content of the supernatant was analyzed by ICP-MS. The relative Fe content decreased to 90% of its original value after 10 minutes of irradiation. The result indicated that Fe ion leakage from the Gd-MSN@uFe-Bt-NPs hybrid was very low in a short irradiation time, which ensures its phototherapeutic effect.

Experimental Part

Combination of Gd-NPs and uFe-NPs

Gadolinium(III) oxide nanoparticles were combined utilizing an aqueous procedure wherein Gd_2O_3 was somewhat diminished preceding the development of Gd_2O_3 -MSN. Quickly, 1500 g of Gd_2O_3 , 2500 g of NaAc, and 1.4 g of SDBS were applied to a mix of 10 mL of EG and 30 mL of DEG. The blend was then vivaciously mixed for 5 hours and fixed in a 50 mL Teflon-lined hardened steel autoclave (with a filling proportion of roughly 70%) at 200°C for 12 hours. Subsequent to chilling off to room temperature, the material was washed multiple times with ethanol and DI air, at that point extricated by attractive partition and dried in a vacuum broiler at 60°C for 24 hours. In the end, APTES was utilized as a wellspring of amino gatherings for the change of Gd-NPs under acidic conditions, and Gd-NPs were acquired by the disposal of free APTES. Gadolinium(III) oxide nanoparticles have been blended by the past strategy utilized.²⁷⁻²⁹

Readiness of Spiral Gd_2O_3 @ SiO_2 Mesoporous (Gd-MSN)

Typically, 1.0 g of Cetyltrimethylammonium Bromide (CTAB) was applied to the arrangement of $\text{NH}_3\bullet\text{H}_2\text{O}$ (2 mL)

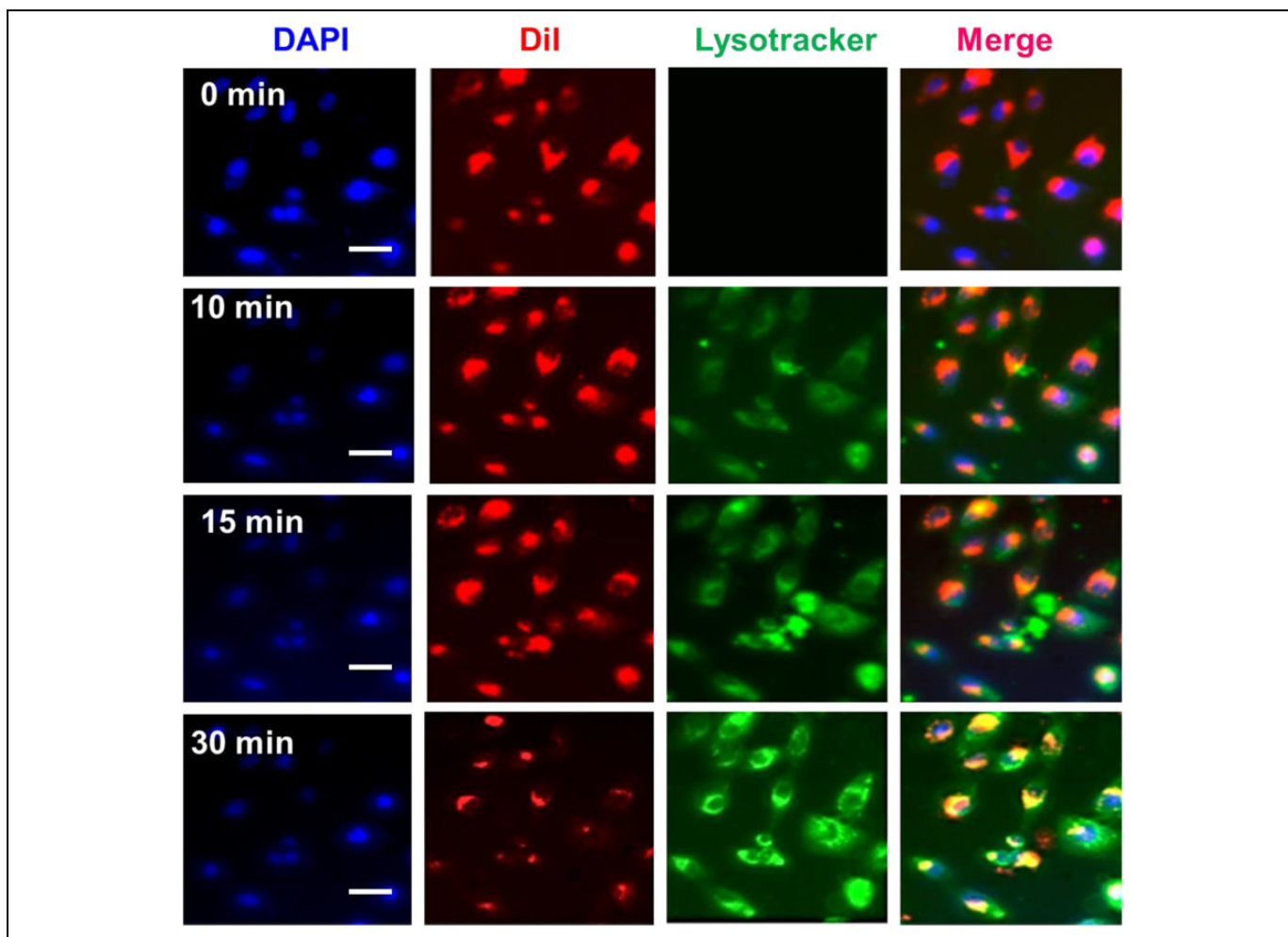


Figure 5. Cellular uptake of Gd-MSN@uFe-Bt-NPs for MCF-7 cells with different time periods (0, 10, 15, and 30 minutes). Scale bar is 10 μ m.

and DI fluid (180 mL). Once CTAB had totally broken up, 35 mL of ether and 50 mL of anhydrous ethanol were included. After bubbling, 0.2 g Gd-NPs, which were homogeneously spread in 10 mL of anhydrous ethanol, were applied to the blend. Later in the wake of mixing for 10 minutes, 5 mL of TEOS was added drop shrewd to the response blend under enthusiastic mixing at room temperature for another 2 hours. The last Gd-MSN-NPs were secluded by attractive partition and washed multiple times with DI water and ethanol and in the end dried at 70°C for 12 hours. In the argon environment, the as-arranged Fe-MSN-NPs were asserted at 500°C for 4 hours to evacuate CTAB.

Preparation of Bt (Biotin) Changed Gd-MSN-NPs (Gd-MSN-Bt-NPs) and uFe-Stacked Gd-MSN-NPs (Gd-MSN@uFe-Bt-NPs)

The change of the outside of Gd-MSN-NPs with Bt was practiced by a cross-linker science process. To put it plainly, 0.3 g of Gd-MSN-NPs was added to 50 mL of anhydrous EtOH containing 1 mL of APTES. In the wake of blending at room

temperature for 24 hours, the blend was altogether washed with ethanol and dried at 80°C to acquire the Gd-MSN-NH₂-NPs. At that point, 300 mg Bt was empowered utilizing EDC (90 mg) and NHS (80 mg) broke up in a DMF-water (27 mL, 3:1, vol/vol) arrangement with blending for 24 hours. Thus, the Gd-MSN-NH₂-NPs (250 mg) are applied to the dynamic Bt arrangement and mixed at room temperature under anhydrous conditions. Finally, the blend was centrifuged and washed with water and ethanol commonly to get the Gd-MSN-Bt-NPs. So as to set up the Gd-MSN@uFe-Bt-NPs, uFe-NPs were added to the Gd-MSN-NH₂-NPs for another 24 hours of blending earlier alteration with Bt.

In Vitro Cytotoxicity Test and Cellular Uptake

L929 and MCF-7 cells were regularly cultured in Dulbecco's modified Eagle medium (DMEM) and Roswell Park Memorial Institute (RPMI) 1640, respectively. The used DMEM and RPMI 1640 were supplemented with 10% fetal bovine serum, 100 U/mL penicillin, and 100 U/mL streptomycin. The cell culture was maintained at 37°C in a 5% CO₂ incubator.

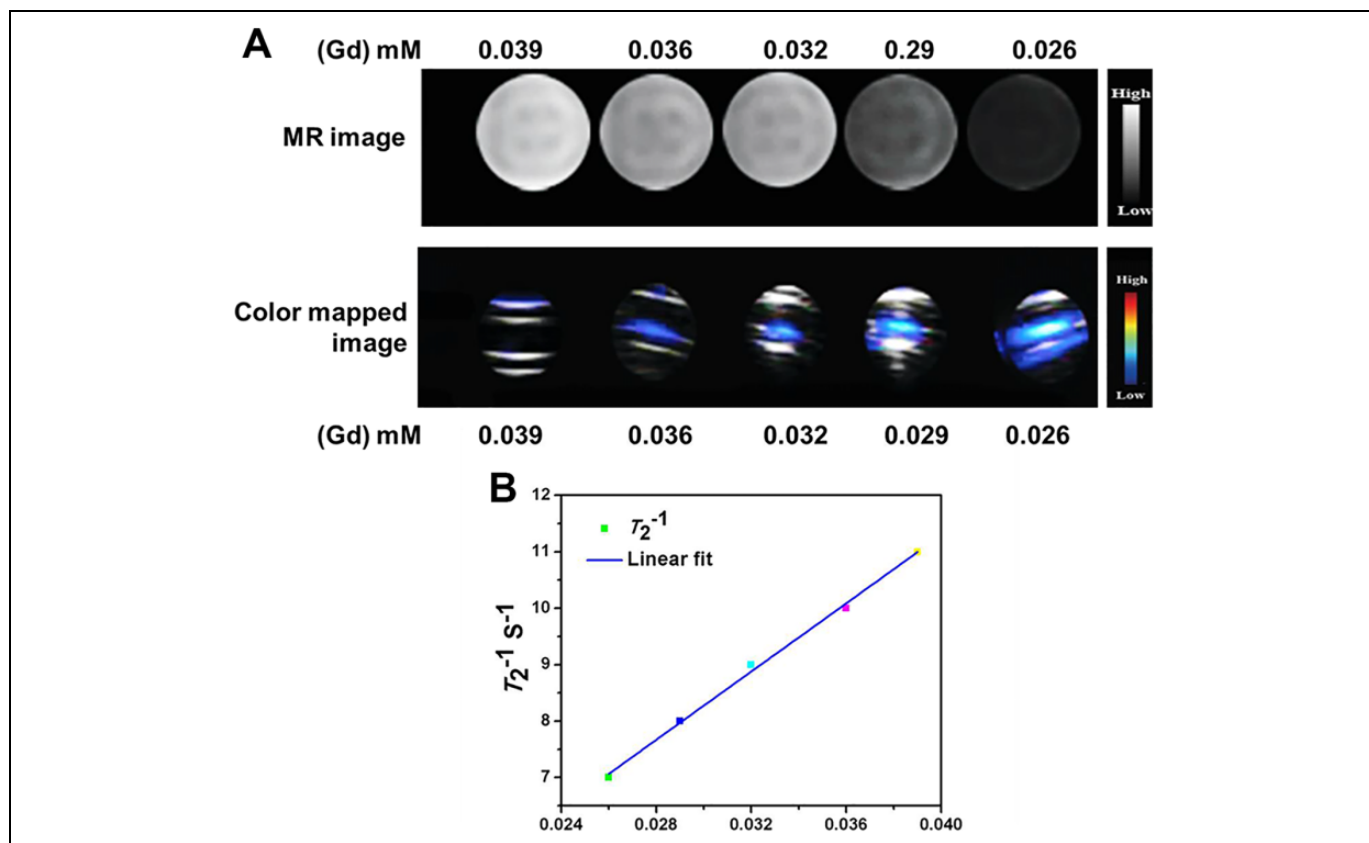


Figure 6. A, In vitro phantom magnetic resonance imaging contrast and color-mapped images of the Gd-MSN@uFe-Bt-NPs at different Gd (mM) concentrations of 0.039, 0.036, 0.032, 0.029, and 0.026. B, Linear fit curve of the T_2 value in relations of various concentrations of Gd (mM).

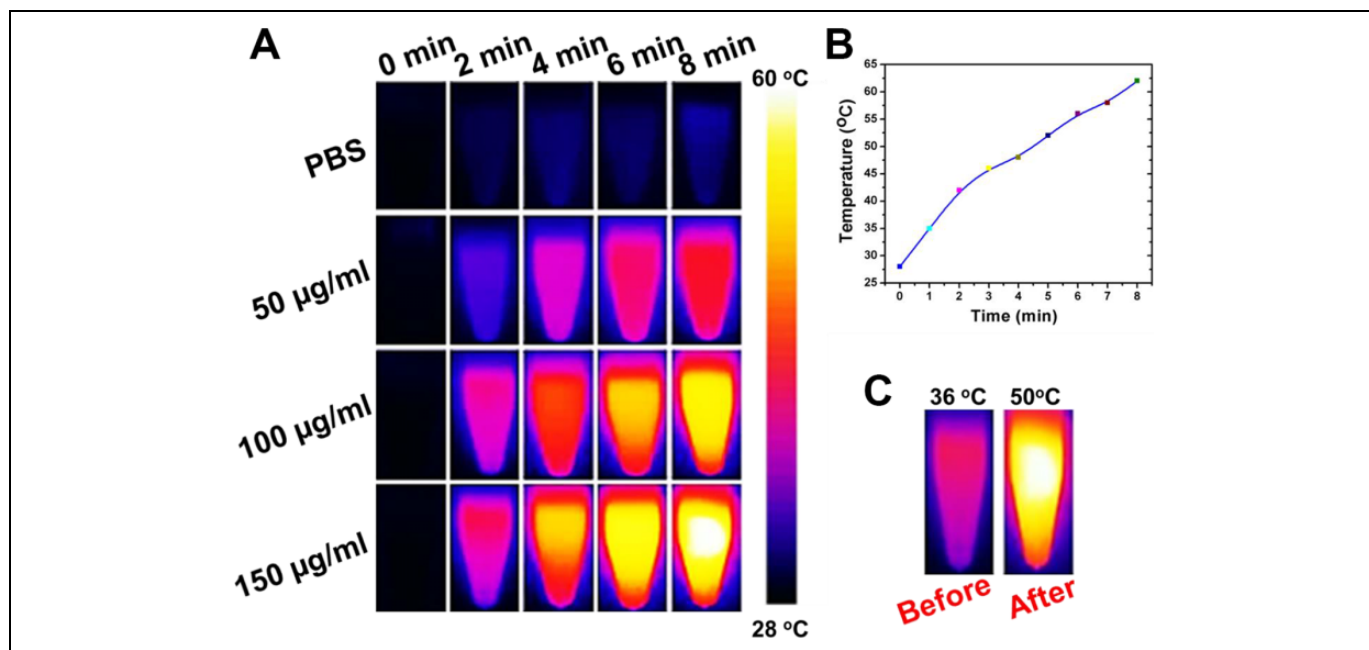


Figure 7. A, The infrared thermal imaging of Gd-MSN@uFe-Bt-NPs with various concentrations. B, The Gd-MSN@uFe-Bt-NPs temperature curve. C, The temperature before and after Gd-MSN@uFe-Bt-NPs.

In brief, 1×10^4 L929 cells were seeded into each well of a 96-well plate with 0.1 mL DMEM and cultured overnight. After that, the medium was replaced with fresh medium containing Gd-MSN@uFe-Bt-NPs, at different Gd concentrations (0, 100, 200, 300, 400, and 500 $\mu\text{g}/\text{mL}$, respectively) for 24 and 48 hours. After that, the medium in each well was discarded and CCK-8 solution (100 μL medium containing 10 μL CCK-8) was added, and the cells were incubated for 4 hours. The MCF-7 cells were seeded into 96-well plate with 0.1 mL of RPMI 1640 and cultured overnight. Next day, the medium was replaced with fresh medium containing Gd-MSN@uFe-Bt-NPs, at different 3.12, 6.25, 12.5, and 50 $\mu\text{g}/\text{mL}$, respectively, for 24 and 48 hours. After that, the medium in each well was discarded and 3-(4,5-Dimethylthiazol-2-yl)-2,5-diphenyltetrazolium bromide (MTT) solution (100 μL medium containing 10 μL MTT) was added and the cells were incubated for 4 hours. Then the absorbance was measured at a wavelength of 450 nm by Thermo Scientific Multiskan MK3 ELISA reader (Thermo Scientific, Waltham, Massachusetts).

MCF-7 cells were seeded in 48-well plates at a density of 2×10^5 cells per well in 1 mL of RPMI 1640 and incubated at 37°C and 5% CO_2 overnight. Next day, the medium was substituted by 1 mL of fresh RPMI 1640 containing Gd-MSN@uFe-Bt-NPs at different time durations (0, 10, 15, and 30 minutes). After 4-hour incubation, the cell number of each well was counted and then the cells were digested by aqua regia solution for 4 hours.³⁰⁻³³

T_2 MR Relaxometry

It is established that Gd-MSN@uFe-Bt-NPs was performed on a 0.5-T NMI20 NMR analyzing and imaging instrument (Niumag, Shanghai, China) at room temperature. The test parameters were set as follows: IR sequence, point resolution of 156 mm \times 156 mm, section thickness of 0.8 mm, and excitation number of 1. The above samples with different Gd concentrations (0.026, 0.029, 0.032, 0.036, and 0.039 mM, respectively) were measured. Besides, the T_2 MR images of the above 3 materials were recorded using a clinical MR system (3.0 T, MAGNETOM VERIO; Siemens Medical Systems, Erlangen, Germany).³⁴⁻³⁷

In Vitro IR Thermal Imaging

The photothermal conversion effect of the hybrid was the main basis of this study. To examine the photothermal conversion effect under 2-photon laser irradiation, 50, 100, and 150 $\mu\text{g}/\text{mL}$ of the Gd-MSN@uFe-Bt-NPs dispersion ($1.0 \times 10^4 \text{ mol}\cdot\text{L}^{-1}$) was stored in vials. An 808 nm laser ($1.5 \text{ W}\cdot\text{cm}^{-2}$) was used as a source for irradiation. The IR thermographic maps and the maximum temperature were captured during 10 minutes of irradiation using a Fluke Ti32 (IR) thermal imaging camera.³⁸⁻⁴⁰

Conclusions

In summary, Gd-MSN@uFe-Bt-NPs with MRI contrast property, active targeting agents, and stimulus response behaviors

have been effectively synthesized via a simple soft-template process for effective breast cancer therapy. Synthesized Gd-MSN@uFe-Bt-NPs displayed high drug loading performance and AMF stimulus response release properties due to high outer surface size of their nanostructure and induced heating properties. In vitro MRI capacities showed a good MRI contrast agents with an extraordinary relaxation value of 299 $\text{Mm}^{-1}\cdot\text{s}^{-1}$. Lastly, in vitro studies have shown that Gd-MSN@uFe-Bt-NPs has countless possibility to act as an MRI-guided stimulus-mediated drug conveyance mechanism aimed at successful active breast cancer therapy.


Declaration of Conflicting Interests

The author(s) declared no potential conflicts of interest with respect to the research, authorship, and/or publication of this article.

Funding

The author(s) received no financial support for the research, authorship, and/or publication of this article.

ORCID iD

Xiaofeng Sun  <https://orcid.org/0000-0003-2540-6720>

References

1. Fiero MH, Roydhouse JK, Vallejo J, King-Kallimanis BL, Kluetz PG, Sridhara R. US Food and Drug Administration review of statistical analysis of patient-reported outcomes in lung cancer clinical trials approved between January, 2008, and December, 2017. *Lancet Oncol.* 2019;20(10):e582-e589. doi:10.1016/s1470-2045(19)30335-3.
2. Mog SR, Zang YJ. Safety assessment of food additives: case example with myrcene, a synthetic flavoring agent. *Toxicol Pathol.* 2019;47(8):1035-1037. doi:10.1177/0192623319879634.
3. Li RJ, Jin R, Liu C, et al. FDA approval summary: calaspargase pegol-mknl for treatment of acute lymphoblastic leukemia in children and young adults. *Clin Cancer Res.* 2019. doi:10.1158/1078-0432.ccr-19-1255.
4. Wedam S, Fashoyin-Aje L, Bloomquist E, et al. FDA approval summary: palbociclib for male patients with metastatic breast cancer. *Clin Cancer Res.* 2019. doi:10.1158/1078-0432.ccr-19-2580.
5. Shu P, Zhao T, Wen B, et al. Application of an innovative high-throughput liquid chromatography-tandem mass spectrometry method for simultaneous analysis of 18 hazardous drugs to rule out accidental acute chemotherapy exposures in health care workers. *J Oncol Pharm Pract.* 2019. doi:10.1177/1078155219870591.
6. Hess LM, Brnabic A, Mason O, Lee P, Barker S. Relationship between progression-free survival and overall survival in randomized clinical trials of targeted and biologic agents in oncology. *J Cancer.* 2019;10(16):3717-3727. doi:10.7150/jca.32205.
7. Xu J, Xie L, Sun X, Dong S, Tang X, Guo W. Management of recurrent or refractory Ewing sarcoma: a systematic review of phase II clinical trials in the last 15 years. *Oncol Lett.* 2019; 18(1):348-358. doi:10.3892/ol.2019.10328.

8. Xiao B, Wang W, Zhang D. Risk of bleeding associated with antiangiogenic monoclonal antibodies bevacizumab and ramucirumab: a meta-analysis of 85 randomized controlled trials. *Oncotargets Ther.* 2018;11:5059-5074. doi:10.2147/OTT.S166151.
9. Tapeinos C, Battaglini M, Ciofani G. Advances in the design of solid lipid nanoparticles and nanostructured lipid carriers for targeting brain diseases. *J Control Release.* 2017;264:306-332. doi:10.1016/j.jconrel.2017.08.033.
10. Goyal SN, Prajapati CP, Gore PR, et al. Therapeutic potential and pharmaceutical development of thymoquinone: a multitargeted molecule of natural origin. *Front Pharmacol.* 2017;8:656. doi:10.3389/fphar.2017.00656.
11. Savla R, Garbuzenko OB, Chen S, Rodriguez-Rodriguez L, Minko T. Tumor-targeted responsive nanoparticle-based systems for magnetic resonance imaging and therapy. *Pharm Res.* 2014;31(12):3487-3502. doi:10.1007/s11095-014-1436-x.
12. Taqanaki ER, Heidari R, Monfared M, Tayebi L, Azadi A, Farjadian F. EDTA-modified mesoporous silica as supra adsorbent of copper ions with novel approach as an antidote agent in copper toxicity. *Int J Nanomedicine.* 2019;14:7781-7792. doi:10.2147/IJN.S218760.
13. Song H, Liu Z, Gai H, et al. Nitrogen-doped ordered mesoporous carbon anchored Pd nanoparticles for solvent free selective oxidation of benzyl alcohol to benzaldehyde by using O₂. *Front Chem.* 2019;7:458. doi:10.3389/fchem.2019.00458.
14. Singh RK, Patel KD, Mahapatra C, Parthiban SP, Kim TH, Kim HW. Combinatory cancer therapeutics with nanoceria-capped mesoporous silica nanocarriers through pH-triggered drug release and redox activity. *ACS Appl Mater Interfaces.* 2019;11(1):288-299. doi:10.1021/acsami.8b17958.
15. Cai D, Liu L, Han C, et al. Cancer cell membrane-coated mesoporous silica loaded with superparamagnetic ferroferric oxide and paclitaxel for the combination of chemo/magnetocaloric therapy on MDA-MB-231 cells. *Sci Rep.* 2019;9(1):14475. doi:10.1038/s41598-019-51029-8.
16. Saini K, Prabhuraj RS, Bandyopadhyaya R. Development of mesoporous silica nanoparticles of tunable pore diameter for superior gemcitabine drug delivery in pancreatic cancer cells. *J Nanosci Nanotechnol.* 2020;20(5):3084-3096. doi:10.1166/jnn.2020.17381.
17. Barkat A, Beg S, Panda SK, Alharbi KS, Rahman M, Ahmed FJ. Functionalized mesoporous silica nanoparticles in anticancer therapeutics. *Semin Cancer Biol.* 2019. doi:10.1016/j.semcancer.2019.08.022.
18. Zhao Z, Chang F, Wang T, et al. Facile assembly of bifunctional, magnetically retrievable mesoporous silica for enantioselective cascade reactions. *Chem Commun (Camb).* 2019;55(90):13578-13581. doi:10.1039/c9cc07123 g.
19. Deng Y, Yue Q, Sun J, Kang Y. Recent advance in interfacial assembly growth of mesoporous silica on magnetite particles. *Angew Chem Int Ed Engl.* 2019. doi:10.1002/anie.201911690.
20. Alphan ery E. Iron oxide nanoparticles for therapeutic applications. *Drug Discov Today.* 2019. doi:10.1016/j.drudis.2019.09.020.
21. Sundar S, Kwon SJ, Venkatachalam G. Magneto-biosensor for the detection of uric acid using citric acid-capped iron oxide nanoparticles. *J Nanosci Nanotechnol.* 2020;20(4):2144-2153. doi:10.1166/jnn.2020.17313.
22. Wang J, Zhang B, Yang G, Su L, Wang L, Gao F. Transferrin-conjugated superparamagnetic iron oxide nanoparticles as in vivo magnetic resonance imaging contrast agents. *J Nanosci Nanotechnol.* 2020;20(4):2018-2024. doi:10.1166/jnn.2020.17311.
23. Pillarisetti S, Uthaman S, Huh KM, Koh YS, Lee S, Park IK. Multimodal composite iron oxide nanoparticles for biomedical applications. *Tissue Eng Regen Med.* 2019;16(5):451-465. doi:10.1007/s13770-019-00218-7.
24. Wang B, Gu L, Zhang D, Wang WA. High-throughput production of Zr-doped Li₄ Ti₅ O₁₂ modified by mesoporous Libaf₃ nanoparticles for superior lithium and potassium storage. *Chem Asian J.* 2019;14(18):3181-3187. doi:10.1002/asia.201900873.
25. Shen Y, Gong S, Li J, et al. Co-loading antioxidant N-acetylcysteine attenuates cytotoxicity of iron oxide nanoparticles in hypoxia/reoxygenation cardiomyocytes. *Int J Nanomedicine.* 2019;14:6103-6115. doi:10.2147/IJN.S209820.
26. Zhang Y, Li J, Li W, Kang D. Synthesis of one-dimensional mesoporous Ag nanoparticles-modified TiO₂ nanofibers by electrospinning for lithium ion batteries. *Materials (Basel).* 2019;12(16). doi:10.3390/ma12162630.
27. Loai Y, Ganesh T, Cheng HL. Concurrent dual contrast for cellular magnetic resonance imaging using gadolinium oxide and iron oxide nanoparticles. *Int J Mol Imaging.* 2012;2012:230942. doi:10.1155/2012/230942.
28. Bridot JL, Faure AC, Laurent S, et al. Hybrid gadolinium oxide nanoparticles: multimodal contrast agents for in vivo imaging. *J Am Chem Soc.* 2007;129(16):5076-5084. doi:10.1021/ja068356j.
29. Mortezaazadeh T, Gholibegloo E, Alam NR, et al. Gadolinium (III) oxide nanoparticles coated with folic acid-functionalized poly(β -cyclodextrin-co-pentetic acid) as a biocompatible targeted nano-contrast agent for cancer diagnostic: in vitro and in vivo studies. *MAGMA.* 2019;32(4):487-500. doi:10.1007/s10334-019-00738-2.
30. Tang S, Wang A, Yan X, et al. Brain-targeted intranasal delivery of dopamine with borneol and lactoferrin co-modified nanoparticles for treating Parkinson's disease. *Drug Deliv.* 2019;26(1):700-707. doi:10.1080/10717544.2019.1636420.
31. Sun F, Zheng Z, Lan J, et al. New micelle myricetin formulation for ocular delivery: improved stability, solubility, and ocular anti-inflammatory treatment. *Drug Deliv.* 2019;26(1):575-585. doi:10.1080/10717544.2019.1622608.
32. Li L, He S, Yu L, et al. Codelivery of DOX and siRNA by folate-biotin-quaternized starch nanoparticles for promoting synergistic suppression of human lung cancer cells. *Drug Deliv.* 2019;26(1):499-508. doi:10.1080/10717544.2019.1606363.
33. Mahmoud NN, Al-Kharabsheh LM, Khalil EA, Abu-Dahab R. Interaction of gold nanorods with human dermal fibroblasts: cytotoxicity, cellular uptake, and wound healing. *Nanomaterials (Basel).* 2019;9(8). doi:10.3390/nano9081131.
34. Samiei Foroushani M, Niroumand N, Karimi Shervedani R, Yaghoobi F, Kefayat A, Torabi M. A theranostic system based on nanocomposites of manganese oxide nanoparticles and a pH sensitive polymer: Preparation, and physicochemical

- characterization. *Bioelectrochemistry*. 2019;130:107347. doi:10.1016/j.bioelechem.2019.107347.
35. Vu-Quang H, Vinding MS, Jakobsen M, et al. Imaging rheumatoid arthritis in mice using combined near infrared and ^{19}F magnetic resonance modalities. *Sci Rep*. 2019;9(1):14314. doi:10.1038/s41598-019-50043-0.
36. Pan X, Lie AL, White TW, Donaldson PJ, Vaghefi E. Development of an in vivo magnetic resonance imaging and computer modelling platform to investigate the physiological optics of the crystalline lens. *Biomed Opt Express*. 2019;10(9):4462-4478. doi:10.1364/BOE.10.004462.
37. Hannecart A, Stanicki D, Vander Elst L, et al. Embedding of superparamagnetic iron oxide nanoparticles into membranes of well-defined poly(ethylene oxide)-block-poly(ϵ -caprolactone) nanoscale magnetovesicles as ultrasensitive MRI probes of membrane bio-degradation. *J Mater Chem B*. 2019;7(30):4692-4705. doi:10.1039/c9tb00909d.
38. Zhang T, Jiang Z, Xue T, et al. One-pot synthesis of hollow PDA@DOX nanoparticles for ultrasound imaging and chemothermal therapy in breast cancer. *Nanoscale*. 2019;11(45):21759-21766. doi:10.1039/c9nr05671h.
39. Gu W, Zhang T, Gao J, et al. Albumin-bioinspired iridium oxide nanoplatform with high photothermal conversion efficiency for synergistic chemo-photothermal of osteosarcoma. *Drug Deliv*. 2019;26(1):918-927. doi:10.1080/10717544.2019.1662513.
40. Qiu Y, Ding D, Sun W, et al. Hollow mesoporous carbon nanospheres for imaging-guided light-activated synergistic thermochemotherapy. *Nanoscale*. 2019;11(35):16351-16361. doi:10.1039/c9nr04802b.